

Unified description for the nuclear equation of state and fragmentation in heavy-ion collisions

Jicai Pan and Subal Das Gupta

Department of Physics, McGill University, 3600 University St., Montréal, Québec, Canada H3A 2T8

(Received 27 July 1994; revised manuscript received 19 October 1994)

We propose a model that provides a unified description of the nuclear equation of state and fragmentations. The equation of state is evaluated in the Bragg-Williams as well as in the Bethe-Peierls approximations and compared with that in the mean field theory with Skyrme interactions. The model shows a liquid-gas type phase transition. The nuclear fragment distributions are studied for different densities at finite temperatures. Power law behavior for fragments is observed at the critical point. The study of the fragment distribution and the second moment S_2 shows that the thermal critical point coincides with the percolation point at the critical density. High temperature behavior of the model shows characteristics of chemical equilibrium.

PACS number(s): 25.70.-z, 24.60.-k, 05.50.+q, 05.70.-a

I. INTRODUCTION

The phenomenon of nuclear matter fragmenting into various pieces can be studied in heavy-ion collisions. This has been an area of much activity, both in experiments and in theory. Curtin, Toki, and Scott [1] pointed out that at some incident energies excited matter that is formed in heavy-ion collisions will pass through a liquid-gas phase transition stage, and if fragments are formed at this stage, it may show characteristics of this transition. A study of nuclear matter with a Skyrme interaction was made in [2] where it was shown that in mean field theory there is a phase transition as in the van der Waals gas. In nuclear physics, a phase transition, if it indeed happens, is a transient phenomenon and it is not clear what the mean field theory predicts for observables that can actually be measured. In experiments the most readily accessible observable is the cross section of nuclear fragments or yield $Y(A)$ vs A , where A is the mass number or charge of a fragment. Of course mean field theories cannot make a prediction about the fragment distribution and thus they fall short of directly providing results with which one could confront the data.

Bauer *et al.* [3] and Campi and Debois [4] used the percolation model [5] to calculate the fragment distribution [6,7]. There are two varieties of percolation models: the bond and the site percolation models. In a bond percolation model each site of the lattice is occupied by a nucleon. That is, the number of nucleons equals the number of lattice sites, N . The bonds between nearest neighbors are broken with a probability of $1 - p$ where p is the probability that the bond is unbroken. Nucleons which are connected through unbroken bonds form a cluster. In a site percolation model, each site is occupied randomly with probability $p \leq 1$. The number of nucleons, n , is usually less than or equal to the number of the lattice sites, N . Nucleons occupying nearest neighbor sites are considered to be the part of one cluster. In both bond and site percolation models there is a critical value p_c of p at which an infinite cluster starts to emerge. For a

very large lattice p_c is independent of N . The probability that a given site belongs to this infinite cluster is zero for $p < p_c$, and grows from 0 to 1 for $p \geq p_c$. In general, the cluster distributions in percolation models are very similar to the mass distribution observed in heavy-ion collisions [6,7].

The percolation model is quite different from the mean field theories that we first alluded to. There is just one parameter in a percolation model. In a bond percolation model the number of sites equals the number of nucleons. One might regard that the probability p is a function of temperature. In that case there is no parameter corresponding to the volume or the pressure of the system. If instead one takes the site percolation model, the number of lattice sites, N , is usually larger than n . One may now associate the parameter p with the volume. There is, then, no reference to temperature or pressure. Thus the simple percolation model cannot describe the thermodynamic aspect of nuclear fragmentation.

Our present work started with the desire to have a model that can describe both the equation of state and the fragmentation of finite nuclear systems. The quintessence of this model is the lattice gas model [8]. The model leads to a (P, V, T) diagram, and it is also linked with the percolation model in an obvious way. An interesting feature is that it not only leads to a liquid-gas type of phase transition, but also encompasses the percolation transition.

Much work has been published on the subject of the liquid-gas phase transition in nuclei. See Refs. [9–11] for a description of some early works and [12] for a review. There are microscopic models which are proposed to calculate multifragmentation [13–17]. Other phenomenological models can be found in [18]. The pioneering work by the Purdue group [19] was a big impetus for this subject.

II. MODEL

We consider the participant zone in collisions of two heavy-ions and conjecture that because of nucleon-

nucleon collisions the system reaches thermal equilibrium. We assume that the system is adequately described by classical statistical mechanics. In that case the canonical partition function of an n -particle system can be written in a separable form: $Z_{\text{can}} \propto Z_p(\text{can})Z_r(\text{can})$ where $Z_p(\text{can})$ is given by

$$Z_p(\text{can}) = \int \exp \left[-\beta \sum_1^n p_i^2/2m \right] d^3p_1 \cdots d^3p_n, \quad (2.1)$$

where β is the inverse temperature. The other part of the partition function is

$$Z_r(\text{can}) \propto \int \exp \left[-\beta \sum_{i<j} v(r_{ij}) \right] d^3r_1 \cdots d^3r_n. \quad (2.2)$$

Here $v(r_{ij})$ is the potential between particles i and j . We approximate the configuration part of the partition function by the partition function of the lattice gas model. In this model (as in a site percolation model) each lattice site can be occupied by at most one nucleon. The number of lattice sites, N , gives a measure of the volume of the system and is usually larger than n . When the nucleus is in the ground state we have $n = N$. Thus our model is limited to a normal nuclear volume or higher. Because cluster formation presumably takes place at a volume much larger than the normal volume, this restriction may not be a debilitating factor. In contrast with the percolation model, the lattice gas model includes interactions. If two nearest neighboring sites are filled by nucleons, they will interact and the energy of interaction is denoted by $-\epsilon$. The nearest neighbor interaction simulates the short range nature of the nucleon-nucleon interaction.

We can now write down the canonical partition function for our model for a fixed n and N . The $Z_p(\text{can})$ is simple and does not depend on the volume, and we just need to calculate the $Z_r(\text{can})$. Let N_{nn} be the number of nn bonds in a specific lattice configuration; the energy carried by these bonds is then $-\epsilon N_{nn}$. Then $Z_r(\text{can})$ is given by

$$Z_r(\text{can}) = \sum_{N_{nn}} g(N, n, N_{nn}) e^{\beta \epsilon N_{nn}}, \quad (2.3)$$

where $g(N, n, N_{nn})$ is a degeneracy factor satisfying

$$\sum_{N_{nn}} g(N, n, N_{nn}) = \frac{N!}{(N-n)!n!}. \quad (2.4)$$

An exact evaluation of $Z_r(\text{can})$ given in (2.3) is difficult. Thus we will use approximate means.

III. EQUATION OF STATE

A. Bragg-Williams approximation

The Bragg-Williams approximation is an easy and quick calculation but is not expected to be accurate.

The results are, however, transparent and analytically demonstrate van der Waals type behavior. In this approximation the number of nn bonds, N_{nn} , is taken to be given and fixed, when N and n are specified. If one site is definitely occupied, the number of its γ neighbors that are occupied is on the average $\gamma n/N$. In our three-dimensional simple cube lattice γ is 6 except at the boundary. Since there are n nucleons in the system, the number of nn bonds is then $\gamma n^2/2N$ where we have ensured that each bond is only counted once and assumed that both n and N are large so that boundary effects can be neglected. In the Bragg-Williams approximation the canonical partition function is then

$$Z_r(\text{can}) = \frac{N!}{(N-n)!n!} e^{\frac{1}{2}\beta\epsilon\gamma\frac{n^2}{N}}. \quad (3.1)$$

The equation of state can be calculated by utilizing $P = kT[\partial \ln Z(\text{can})/\partial V]_T = kT[\partial \ln Z_r(\text{can})/\partial V]_T$ since $Z_p(\text{can})$ does not have any V dependence. Here P is the pressure and V is the volume given by $V = a^3 N$. A representative value of a^3 would be $a^3 = 1/\rho_0 = 6.25 \text{ fm}^3$ where ρ_0 is the normal nuclear density. The normal nuclear volume is $V_0 = a^3 n$. Using Stirling's approximation for $N!$, $n!$, and $(N-n)!$ one can show that

$$P = \frac{kT}{a^3} \ln \frac{N}{N-n} - \frac{1}{2a^3} \epsilon \gamma \left(\frac{n}{N} \right)^2. \quad (3.2)$$

Using $n/N = V_0/V = \rho/\rho_0$ we finally get

$$P = kT\rho_0 \ln \left(\frac{V}{V-V_0} \right) - \frac{1}{2} \epsilon \rho_0 \gamma \left(\frac{V_0}{V} \right)^2. \quad (3.3)$$

This equation of state has the same qualitative behavior as the van der Waals gas. For 1 mol of gas, the van der Waals equation of state is

$$P = \frac{N_A kT}{V-b} - \frac{a}{V^2}. \quad (3.4)$$

The lattice gas pressure goes to infinity as V approaches V_0 . The van der Waals gas pressure goes to infinity as V is squeezed to the value b . For large V both equations of state approach the perfect gas limit. The critical point can be readily determined analytically from (3.3). By setting $\partial P/\partial \rho = \partial^2 P/\partial \rho^2 = 0$ at the critical point we obtain $\rho_C = 0.5\rho_0$ and $kT_C = \gamma\epsilon/4$, respectively. It is also straightforward to show that in the Bragg-Williams approximation $P_C V_C / RT_C = 2 \ln 2 - 1 = 0.386$ for the lattice gas. The corresponding number for the van der Waals gas is 0.375.

The Bragg-Williams approximation is considered to be crude and one may wonder if the lattice gas model would indeed lead to a liquid-gas type phase transition when a better mean field calculation is done. In the next subsection we try an improved approximation.

B. Bethe-Peierls approximation

We now try to do a better mean field calculation and use what is called the Bethe-Peierls approximation in the Ising model. For the Ising model, the order parameter can be computed without having to calculate the partition function but for the equation of state that we wish to calculate we will need to obtain the partition function. Here we consider a grand canonical ensemble. To explain the methodology we refer to Fig. 1 where, for simplicity, a two-dimensional square lattice is shown. We break up the lattices into $N/(\gamma+1)$ blocks, each of which contains $\gamma+1$ sites. The interactions within each block are treated exactly while the interactions between different blocks are taken into account approximately. The local correlations are taken into account in this approximation, and it is an improvement over the Bragg-Williams approximation. The grand partition function can be written as the product of the grand partition functions of the $N/(\gamma+1)$ blocks:

$$Z_{\text{gr}} = z_{\text{gr}}(\text{block 1})z_{\text{gr}}(\text{block 2}) \cdots z_{\text{gr}}\left(\text{block } \frac{N}{\gamma+1}\right). \quad (3.5)$$

The grand partition function of the block labeled by 1, 2, 3, γ , and 5 can be written as

$$z_{\text{gr}} = \sum_{k=0}^{\gamma+1} \sum_{\alpha} e^{\lambda'k} e^{-\beta E_{\alpha}(k)}. \quad (3.6)$$

Here λ' plays the role of a chemical potential. The energy $E_{\alpha}(k)$ consists of two parts: the kinetic energy ($\sum_{i=1}^k p_i^2/2m$) and the potential energy for the nearest neighbor interaction. Integration over the kinetic energy part can be immediately done to give a factor of $[(2\pi m/\beta)^{3/2}]^k \equiv e^{qk}$. We now define $\lambda = \lambda' + q$ and also divide the the right hand side of the above equation into two parts:

$$z_{\text{gr}} = \sum_{k=0}^{\gamma} \binom{\gamma}{k} e^{\lambda k + \beta k \bar{\epsilon}} + e^{\lambda} \sum_{k=0}^{\gamma} \binom{\gamma}{k} e^{\lambda k + \beta k (\epsilon + \bar{\epsilon})}. \quad (3.7)$$

The first part is proportional to the probability that site

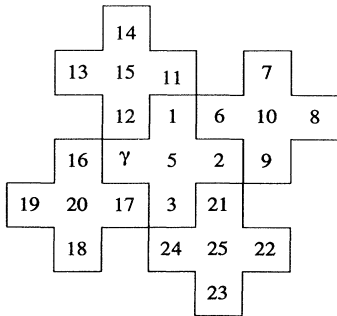


FIG. 1. A square lattice is divided into blocks to illustrate the Bethe-Peierls approximations. See text for details.

5 is unoccupied and its neighboring sites $1 \cdots \gamma$ are k -fold occupied where k goes from 0 to γ . The second part is proportional to the probability that site 5 is occupied where an extra amount of energy $-k\epsilon$ is included when k of the nearest neighbors is also occupied. The extra factor $\exp[\beta k \bar{\epsilon}]$ takes into account the interaction between different blocks. If we left this factor out, the nucleon at site 1 (Fig. 1) would only interact with the one at site 5.

Because of the self-consistency condition, the average occupation probability at every site must be the same. The average occupation at site 5 is

$$P(5) = \frac{e^{\lambda}(1 + e^{\lambda + \beta \epsilon + \beta \bar{\epsilon}})^{\gamma}}{z_{\text{gr}}} = \frac{n}{N}, \quad (3.8)$$

where

$$z_{\text{gr}} = (1 + e^{\lambda + \beta \bar{\epsilon}})^{\gamma} + e^{\lambda}(1 + e^{\lambda + \beta \epsilon + \beta \bar{\epsilon}})^{\gamma} \quad (3.9)$$

is obtained from (3.7) by summing over k . The average number of particles in all the sites neighboring site 5 is

$$\sum_{i=1}^{\gamma} P(i) = \frac{\sum \binom{\gamma}{k} k e^{\lambda k + \beta k \bar{\epsilon}} + e^{\lambda} \sum \binom{\gamma}{k} k e^{\lambda k + \beta k \epsilon + \beta k \bar{\epsilon}}}{z_{\text{gr}}}. \quad (3.10)$$

The self-consistency condition then implies

$$e^{\lambda}(1 + e^{\lambda + \beta \epsilon + \beta \bar{\epsilon}})^{\gamma} = e^{\lambda + \beta \bar{\epsilon}}(1 + e^{\lambda + \beta \bar{\epsilon}})^{\gamma-1} + e^{2\lambda + \beta(\epsilon + \bar{\epsilon})}(1 + e^{\lambda + \beta(\epsilon + \bar{\epsilon})})^{\gamma-1}. \quad (3.11)$$

The two unknowns e^{λ} and $\bar{\epsilon}$ can be solved from (3.8), (3.9), and (3.11). Dividing both sides of (3.11) by $e^{\lambda}(1 + e^{\lambda + \beta(\epsilon + \bar{\epsilon})})^{\gamma-1}$, we obtain

$$1 = e^{\beta \bar{\epsilon}} \left[\frac{1 + e^{\lambda + \beta \bar{\epsilon}}}{1 + e^{\lambda + \beta \epsilon + \beta \bar{\epsilon}}} \right]^{\gamma-1}, \quad (3.12)$$

and (3.8) can be rewritten as

$$\frac{N}{n} = 1 + \frac{(1 + \lambda e^{\beta \bar{\epsilon}})^{\gamma}}{e^{\lambda}(1 + e^{\lambda + \beta \epsilon + \beta \bar{\epsilon}})^{\gamma}}. \quad (3.13)$$

Using (3.12), (3.13) becomes

$$\frac{N}{n} = 1 + \frac{1}{e^{\lambda + \beta \bar{\epsilon} \gamma / (\gamma-1)}}. \quad (3.14)$$

We can now write e^{λ} in terms of $\bar{\epsilon}$,

$$e^{\lambda} = \frac{n}{N-n} e^{-\beta \bar{\epsilon} \gamma / (\gamma-1)}. \quad (3.15)$$

Combining (3.8), (3.9), and (3.15) we obtain

$$x = \frac{1}{2} \left[\frac{N-2n}{N-n} + \sqrt{\left(\frac{N-2n}{N-n} \right)^2 + 4 \left(\frac{n}{N-n} \right) e^{\beta \epsilon}} \right], \quad (3.16)$$

where

$$x = e^{\beta\bar{\epsilon}/(\gamma-1)}. \quad (3.17)$$

The values of $\bar{\epsilon}$ and e^λ can now be found from (3.15)–(3.17). We note here that the results depend on the ratios of n/N and ϵ/kT only.

Let us now go back to the partition function for the lattice given in (3.5) where it is written as a product of the partition functions of the $N/(\gamma+1)$ blocks. If we simply use the partition function for each block given in (3.9), we count twice the binding energies between neighboring sites in different blocks. For example, the binding energy between 1 and 6 (Fig. 1) is included in z_{gr} (block 1) through $\bar{\epsilon}$, and it is included again in z_{gr} (block 2). We note that on the average there are n/N particles at each site, and each block has γ peripheral sites. Thus, when we evaluate the partition function for the lattice, the partition function for each block given in (3.9) should be corrected with the following factor:

$$\text{correction} = e^{-\frac{1}{2}\beta\bar{\epsilon}\gamma n/N}. \quad (3.18)$$

We can now use $PV/kT = \ln Z_{gr}$, $V = N/\rho_0$, and $\ln Z_{gr} = N/(\gamma+1) \ln z_{gr}$ to obtain

$$P = \rho_0 kT \frac{1}{\gamma+1} \ln z_{gr}. \quad (3.19)$$

Here z_{gr} is now understood as the product of a block partition function given in (3.9) and the correction factor given in (3.18).

The equations of state calculated in the Bragg-Williams approximation and the Bethe-Peierls approximation are compared in Fig. 2 in P - V diagrams at different temperature. It is seen that in the high temperature limit both give the same results, and they begin to differ at low temperatures.

C. Mean field theory with Skyrme interaction

We take a Skyrme interaction with potential energy density given by [2]

$$V(\rho) = \frac{A}{2} \rho_0 \left(\frac{\rho}{\rho_0} \right)^2 + \frac{B}{\sigma+1} \rho_0 \left(\frac{\rho}{\rho_0} \right)^{\sigma+1}, \quad (3.20)$$

where $A = -356$ MeV, $B = 303$ MeV, and $\sigma=7/6$. This interaction produces a saturation density of 0.16 fm^{-3} and binding energy of 16 MeV per particle.

The pressure consists of two parts: one originating from the interaction and the other from the kinetic energy. The pressure produced by the interaction is given by

$$\left[\frac{A}{2} \frac{\rho}{\rho_0} + \frac{\sigma B}{\sigma+1} \left(\frac{\rho}{\rho_0} \right)^\sigma \right] \rho. \quad (3.21)$$

The kinetic pressure is calculated numerically from a Fermi gas model at finite temperature.

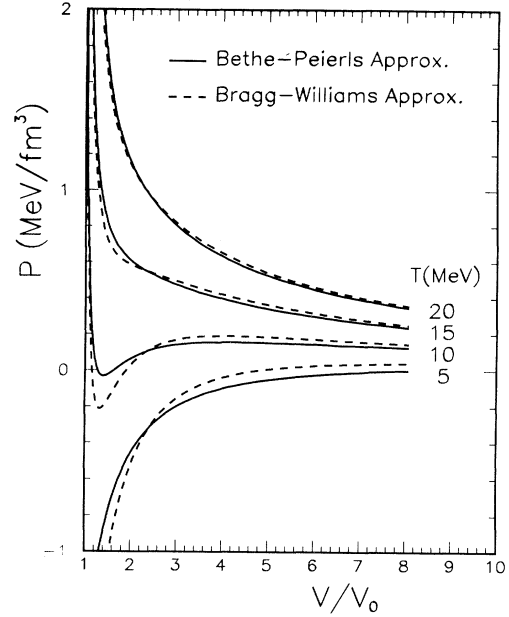


FIG. 2. The P - V diagrams in lattice gas model at temperatures $T = 5, 10, 15,$ and 20 MeV. The solid curves are for the Bethe-Peierls approximation, and the dashed curves are for the Bragg-Williams approximation. In the calculation we used $\epsilon = 9$ MeV.

Similar to Fig. 2 one can draw P against $V/V_0 (= \rho_0/\rho)$ at various T . A comparison of the equation of state in the mean field theory with a Skyrme interaction and in the lattice gas is shown in Fig. 3. In both cases we see characteristics of a liquid-gas phase transition. In the calculation we used $\epsilon=9$ MeV and $\rho_0 = 0.16 \text{ fm}^{-3}$.

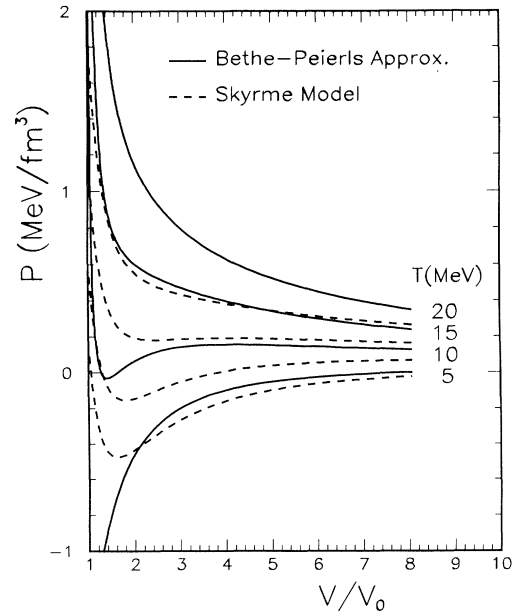


FIG. 3. The same as Fig. 2, but the dashed curves are for the mean field theory with Skyrme interactions.

IV. FRAGMENT DISTRIBUTIONS

Nuclear fragmentations are described by the formation of clusters in our model. To generate fragments we need to simulate the lattice configuration and momenta of particles, and to determine if neighboring particles belong to the same cluster. The lattice configuration is generated according to (2.2), while the momenta are generated from the Maxwell-Boltzmann factor given in (2.1). These two processes are independent of each other since the partition function can be factorized. To generate the configuration we start from an empty lattice and put the first nucleon at random. Once this has been put in, the γ boxes that are immediate neighbors are assigned a probability $\propto \exp[\beta\epsilon]$ whereas all other boxes have probability proportional to unity. The next nucleon is then put in according to this probability distribution. If at an intermediate state there are m empty boxes, we assign to each of these boxes a probability proportional to $\exp[q\beta\epsilon]$ where q is the number of nearest neighbors that are already filled up. The next filling is then done according to this distribution. The difference from the computer simulation that would be done in a site percolation model is the Boltzmann factor. Having done the configuration space sampling we then assign each nucleon a momentum according to the Maxwell-Boltzmann distribution.

In a site percolation model two neighboring particles always form a cluster. The formation of a cluster in our model depends on the interactions of neighboring particles and their relative kinetic energy. We adopt the following physical criterion for determining the formation of a cluster. Two neighboring nucleons belong to the same cluster if the following condition is satisfied:

$$\mathbf{p}_r^2/2\mu - \epsilon < 0. \quad (4.1)$$

Here \mathbf{p}_r is the relative momentum between the two nucleons and μ is the reduced mass. Except at very low temperatures, the frequency with which two nucleons appear at neighboring sites depends mostly on the density. The probability of $\mathbf{p}_r^2/2\mu$ exceeding the value ϵ increases with temperature since the momentum of each nucleon is obtained from Monte Carlo sampling of the Maxwell-Boltzmann distribution. Hence the probability that two nucleons are bonded decreases with increasing temperature and the system becomes less compact at higher temperature as it should. A different parametrization used in [20] leads to similar effects.

We note that when each particle obeys the Maxwell-Boltzmann distribution, the distribution of relative momentum between two particles is also Maxwell-Boltzmann, i.e., $P(\mathbf{p}_r) = [1/(2\pi\mu kT)^{3/2}] \exp[-\mathbf{p}_r^2/2\mu kT]$. We can then write down a formula for the bonding probability which is temperature dependent:

$$p = 1 - \frac{4\pi}{(2\pi\mu kT)^{3/2}} \int_{\sqrt{2\mu\epsilon}}^{\infty} e^{-\mathbf{p}_r^2/2\mu kT} p_r^2 dp_r. \quad (4.2)$$

Coniglio and Klein [22] used a different parametrization for the bonding probability. They used

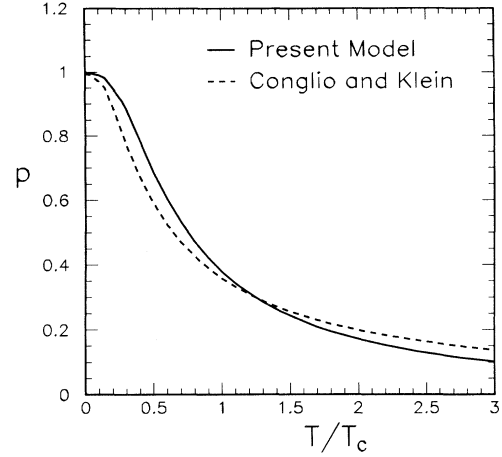


FIG. 4. The bond probability p_B is plotted as a function of temperature. The solid curve is obtained from our model given in Eq. (4.2), and the dashed curve is the Coniglio-Klein model shown in Eq. (4.3).

$$p = 1 - \exp[-\beta\epsilon/2]. \quad (4.3)$$

This was mathematically devised so that the thermal critical point would also be a percolation point, a feature, as we shall see, that is also present in our parametrization. A comparison of the two formulas is presented in Fig. 4. An example of the fragment distribution obtained in our simulation is shown in Fig. 5. One could decipher from this figure that at $T = 0.5T_C$ the system percolates, at $T = 1.5T_C$ and $T = 2.0T_C$ there is no percolation, and that percolation sets in around $T = T_C$.

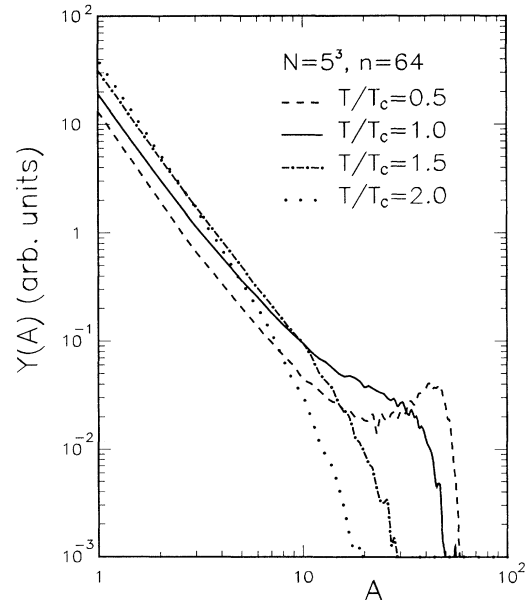


FIG. 5. The mass yield distribution, $Y(A)$ vs A , for lattice $N = 5^3$ and $n = 64$, at temperatures $T/T_C = 0.5, 1.0, 1.5,$ and 2.0 . Here $T_C = 1.1275\epsilon$ is the thermal critical temperature. This value of T_C taken from [24] is more accurate than the Bragg-Williams approximation.

V. THERMAL CRITICAL POINT AND PERCOLATION POINT

Let p_c be the value of p at the percolation point, i.e., the point when an infinite cluster just appears. The cluster size distribution for a general p can be parametrized as [5]

$$Y(A, p) = A^{-\tau} f[(p - p_c)A^\sigma]. \quad (5.1)$$

The scaling function $f(x)$ can be determined by computer simulations or experiments. In many cases, such as the Fisher model [23], $f(x)$ is an exponential function. At the percolation point, the fragment distribution obeys a simple power law

$$Y(A, p_c) \propto A^{-\tau}. \quad (5.2)$$

At the percolation point the fluctuation is the maximum. This means that if in the neighborhood of the percolation point the yield $Y(A, p)$ is fitted by a power law, the exponent τ will be a minimum at the percolation point. Experimental data are often fitted by a power law and a minimum in τ is searched for to ascertain the percolation point [21].

The second moment is defined as $S_2 = \sum A^2 n(A)/n$ where $n(A)$ is the number of clusters with A nucleons and the sum excludes the largest cluster (defined henceforth as A_{\max}). In the thermodynamic limit S_2 diverges at the percolation point and obeys a power law distribution

$$S_2 \propto |p - p_c|^{-\gamma}. \quad (5.3)$$

As mentioned, the order parameter given by $\lim_{n \rightarrow \infty} A_{\max}/n$ is zero for $p < p_c$ and increases with p for $p \geq p_c$. Above the percolation point the order parameter is given by

$$A_{\max}/n \propto |p - p_c|^\beta. \quad (5.4)$$

There are two independent critical exponents in most statistical models and percolation models. One can readily show that the following relations exist:

$$\gamma = \frac{3 - \tau}{\sigma}, \quad (5.5)$$

$$\beta = \frac{\tau - 2}{\sigma}, \quad (5.6)$$

and

$$\tau = 2 + \frac{\beta}{\beta + \gamma}. \quad (5.7)$$

For a finite system the second moment S_2 goes through a maximum (instead of infinity), and τ goes through a minimum at the percolation point. Thus τ and S_2 can be used to identify the percolation point in a finite system.

In our model there is, first of all, a thermal critical point which is obtained at $\rho_C = 0.5\rho_0$ and $T_C = 1.1275\epsilon$ [24]. This more exact value of $T_C = 1.1275\epsilon$ is smaller than the value of 1.5ϵ that we obtained from the Bragg-Williams approximation. But, in addition, there is a continuous range of percolation points. Provided the density

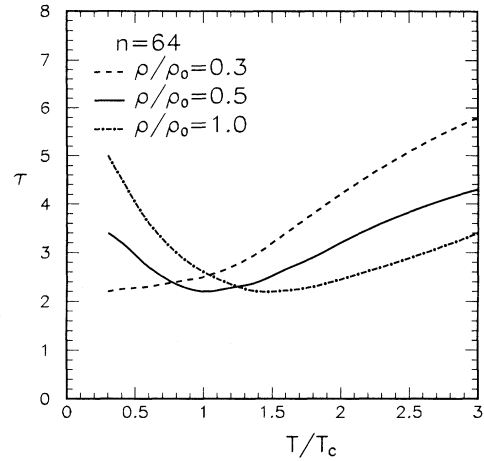


FIG. 6. The value of τ is plotted as a function of temperature at different densities.

is higher than a minimum value ($\approx 0.3\rho_0$) a percolation point will be reached at a certain temperature. The higher the density, the higher the temperature at which percolation sets in. If we identify the point at which a maximum in S_2 or a minimum in τ is achieved as the percolation point, then we see from Figs. 6 and 7 that at higher density the percolation point is reached at a higher temperature. One can now ask the question: If a minimum in τ is seen in experiments as in Ref. [19], one could interpret that as an indication that the percolation point is reached but does it have any relevance with the thermal critical point? As Fig. 7 shows if the freeze-out density is $0.5\rho_0$, then the percolation point is reached at the thermal critical point. It also follows that if the freeze-out density is close to $0.5\rho_0$, then a minimum in τ is obtained when the temperature of the dissociating system is close to the critical temperature.

We therefore have this remarkable result which was not *a priori* imposed. In our model the thermal critical point is also a percolation point. Numerically this result can be

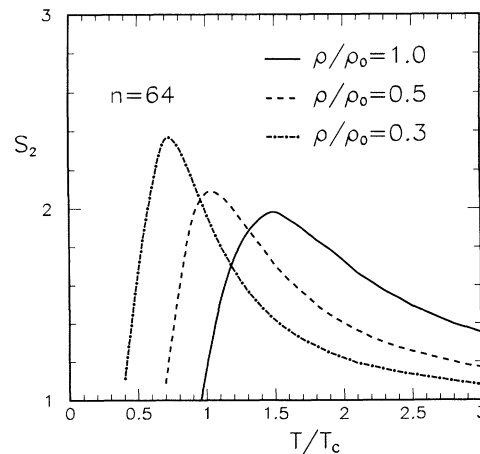


FIG. 7. The value of S_2 is plotted as a function of temperature at different densities.

explained by noting that at the critical temperature the value of p in our model differs little from the Coniglio-Klein parametrization. At a density $\rho/\rho_0=1$, the system begins to percolate at $T = 1.47T_C$ in our model and at $T = 1.55T_C$ in the Coniglio-Klein model.

VI. MULTIPLICITY AS A VARIABLE

The implicit thinking in much of what is presented above is that in nuclear collisions matter is compressed, heated up, and we can talk of a freeze-out density and temperature at the time of dissociation. Both the temperature and the density are, however, not directly measurable. In the past values of $\frac{3}{4}\rho_0$ and lower have been used for the freeze-out density. It is not known accurately. Given that the most easily measurable quantities are the multiplicity (number of charged particles), S_2 , and A_{\max} , we ask: Can we determine the freeze-out density from the multiplicity dependence of S_2 and A_{\max} ? In Figs. 8 and 9 we plot S_2 and A_{\max} as functions of the multiplicity at different densities. In the calculations, at a given density we took a sufficiently large range of temperatures such that we cover the full range of multiplicity. For a given multiplicity both S_2 and A_{\max} can vary from one event to another. What is plotted is the average for a given multiplicity. From Figs. 8 and 9 we can easily see the changes of S_2 and A_{\max} when the density is changed from $0.3\rho_0$ to $0.5\rho_0$. The differences are, however, rather small between density $0.5\rho_0$ and $1.0\rho_0$. Remembering that there will always be uncertainties in experimental data due to contamination from pre-equilibrium particles, spectators, etc., we conclude that it is difficult from these observations alone to determine the freeze-out density accurately. Some other variables might better differentiate between different freeze-out densities.

VII. BEAM ENERGY AS A VARIABLE

Figure 6 shows that it may be possible that the freeze-out density can be determined from the temperature de-

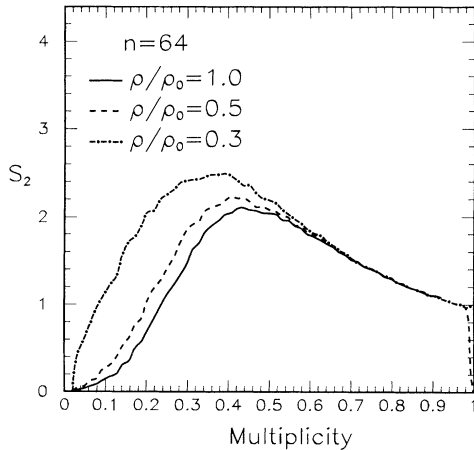


FIG. 8. The value of S_2 is plotted as a function of multiplicity of fragments at different densities.

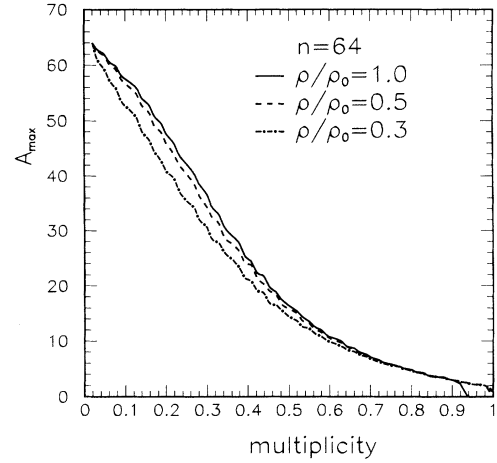


FIG. 9. A_{\max} is plotted as a function of multiplicity of fragments at different densities.

pendence of τ . The temperature is not a direct observable in experiments although it has often been deduced indirectly from other data, notably from slopes of inclusive cross sections. Here we will first try to deduce the temperature from a simple theory so that the temperature is given once the beam energy is given. We consider the experimental setup of [20]. One has nearly central collisions of two nearly equal ions. The experiment is carried out at various beam energies in the laboratory. We take the number of particles to be 85 (corresponding to central $^{40}\text{Ar}+^{45}\text{Sc}$ collisions). In a purely classical model the ground state has no kinetic energy at zero temperature so that the ground state energy per nucleon is $-\epsilon N_{nn}^{\max}/n$ where N_{nn}^{\max} is the maximum number of nn bonds possible for particle number $n = 85$. Since N_{nn}^{\max} is determined by geometry, we can use the experimental binding energy (≈ 8.5 MeV/nucleon) to fix the value of ϵ . At temperature T the average energy per particle is $1.5kT - \epsilon \bar{N}_{nn}/n$ where \bar{N}_{nn} , the average value of N_{nn} , is obtained from computer simulations. We can then write

$$\frac{3}{2}kT + \epsilon(N_{nn}^{\max} - \bar{N}_{nn}) = e^*. \quad (7.1)$$

For equal mass nonrelativistic nuclear collisions we have $e^* = E_{\text{beam}}/4$ where E_{beam} is the beam energy per nucleon in the laboratory. There is an implicit assumption here that all available energy is converted to thermal energy. Thus the temperature is related to the beam energy. We can now fix the freeze-out density at different values, obtain an effective τ at each beam energy, and obtain points as in experiments [20]. This is shown in Fig. 10. However, the fit with data is not good for any of the densities employed.

This type of mapping between beam energy and temperature is not accurate. One of the sources of errors is collective flow which is known to account for some fraction of the available energy. Better mapping could be expected where the temperature is deduced from other experimental data [25,26]. In this approach, the tail of

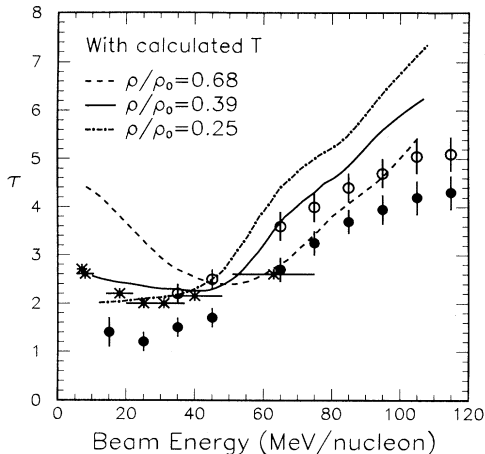


FIG. 10. The theoretical exponent τ is compared with experimental data at different beam energies. The curves are obtained by using the temperature calculated from Eqs. (7.1). The solid circles are the corrected data taken from [21], the open circles are the uncorrected data taken from [20], and the crosses are taken from [26].

the proton cross section is fitted by assuming that the proton has a Maxwell-Boltzmann distribution in a frame which is moving in the laboratory. We take this mapping from [20]. When the mapping from this phenomenological approach is used, the fit with the experimental data is quite good when the freeze-out density is taken to be $0.39\rho_0$ (see Fig. 11). What is also very pleasing is that the predictions for different freeze-out densities are also sufficiently different to be experimentally accessible. The combined study of S_2 and τ as a function of beam energy should be useful in determining the freeze-out density.

VIII. HIGH TEMPERATURE CHARACTERISTICS

Most of the attention in the present work has been focused on temperatures that are close to what is believed to be the critical temperature of nuclear matter. Indeed, in the past the percolation model has mostly been used for mild to moderate excitation energies. At higher energies (i.e., Bevalac energies) other models have been used with moderate success. These models use approximations that are valid in the high-temperature-low-density limits. Chemical equilibrium between different species is assumed. We will call these models by a generic name, the thermodynamic model. In this model rather simple expressions for the average number of monomers (single nucleons \bar{n}_1), dimers (clusters of two nucleons \bar{n}_2), three-body clusters (\bar{n}_3), etc., can be obtained. An early review can be found in [27]. We do not expect to find exact correspondence between these calculations and the present classical model at the high temperature limits since we do not have quantum degeneracies. The clusters in our model consisting of attached cubical boxes in the lattice have degeneracies also. Even for moderate sized

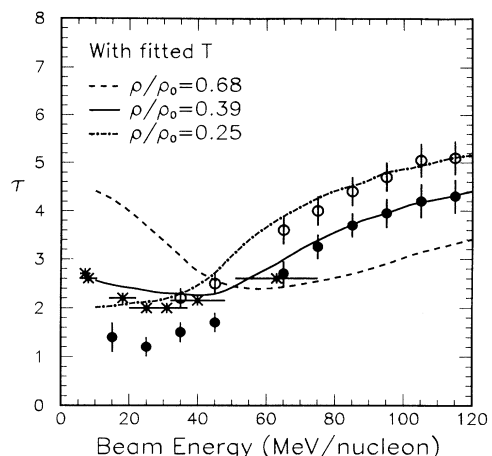


FIG. 11. The same as Fig. 10, but the curves are obtained by using the temperature fitted from experimental data.

clusters these degeneracies require considerable effort to enumerate analytically. Nonetheless, many features seen in experiments are common in both models. For example, in the thermodynamic model, \bar{n}_1 , \bar{n}_2 , and \bar{n}_3 vary with temperature but in a way that $T^{3/2}\bar{n}_2/(\bar{n}_1)^2$ remains constant. Here we have neglected the binding energy of the dimer with respect to kT . Constancy for this ratio is obtained in our present model also. Similarly $\bar{n}_1\bar{n}_3/(\bar{n}_2)^2$ is a constant in both models. The so-called coalescence relation $\frac{d^3\bar{n}_2}{d^3\mathbf{p}}(2\mathbf{p}) \propto [\frac{d^3\bar{n}_1}{d^3\mathbf{p}}(\mathbf{p})]^2$ is obeyed in both models. Thus rather reasonable features emerge when the model is extrapolated to the high temperature side.

IX. SUMMARY

We have presented a model that has links with both mean field aspects and fragmentation of nuclei. We studied the equation of state under different approximations. The model shows a liquid-gas type phase transition. We also studied the nuclear fragmentation and discussed the critical exponents near the critical or percolation points. Some comparisons with experimental data were made.

The purpose of this paper was to present the essentials of this model. The issues we addressed here are far from exclusive. Many other features may be further explored. The present model, we believe, is one step forward from the percolation model which was proved to be helpful for the analysis of experimental data.

ACKNOWLEDGMENTS

We would like to thank H. Guo, C. Gale, J. Kapusta, and M. Grant for useful discussions. This work was supported in part by the Natural Sciences and Engineering Research Council of Canada and by the FCAR fund of the Québec Government.

- [1] M. W. Curtin, H. Toki, and D. K. Scott, *Phys. Lett.* **123B**, 289 (1983).
- [2] H. Jaquaman, A. Z. Mekjian, and L. Zamick, *Phys. Rev. C* **27**, 2782 (1983).
- [3] W. Bauer, D. R. Dean, U. Mosel, and U. Post, in *Proceedings of the Seventh High Energy Heavy Ion Study*, GSI Darmstadt, 1984, GSI Report No. 85-10, 1985, p. 701.
- [4] X. Campi and J. Debois, in *Proceedings of the Seventh High Energy Heavy Ion Study* [3], p. 707.
- [5] D. Stauffer and A. Aharony, *Introduction to Percolation Theory* (Taylor & Francis, London, 1992).
- [6] W. Bauer, *Phys. Rev. C* **38**, 1297 (1988).
- [7] X. Campi, *Phys. Lett. B* **208**, 351 (1988).
- [8] K. Huang, *Statistical Mechanics*, 2nd ed. (John Wiley and Sons, Toronto, 1987).
- [9] D. H. E. Gross, L. Satpathy, T. Meng, and M. Satpathy, *Z. Phys. C* **309**, 42 (1982).
- [10] P. J. Siemens, *Nature* **305**, 410 (1983).
- [11] J. A. Lopez and P. J. Siemens, *Nucl. Phys.* **A431**, 728 (1984).
- [12] L. P. Csernai and J. I. Kapusta, *Phys. Rep.* **131**, 223 (1986).
- [13] W. Bauer, G. F. Bertsch, and S. Das Gupta, *Phys. Rev. Lett.* **58**, 863 (1987).
- [14] J. Gallego, S. Das Gupta, C. Gale, S. J. Lee, C. Pruneau, and S. Gilbert, *Phys. Rev. C* **44**, 463 (1991).
- [15] Ph. Chomaz, G. F. Burgio, and J. Randrup, *Phys. Lett. B* **254**, 340 (1991).
- [16] D. H. E. Gross and B. H. Sa, *Nucl. Phys.* **A437**, 643 (1985); H. R. Jaquaman and D. H. E. Gross, *ibid.* **A524**, 321 (1991).
- [17] S. Ayik and C. Gregoire, *Nucl. Phys.* **A513**, 187 (1990).
- [18] K. C. Chase and A. Z. Mekjian, *Phys. Rev. C* **49**, 2164 (1994).
- [19] J. E. Finn *et al.*, *Phys. Rev. Lett.* **49**, 1321 (1982).
- [20] T. Li *et al.*, *Phys. Rev. C* **49**, 1630 (1994).
- [21] T. Li *et al.*, *Phys. Rev. Lett.* **70**, 1924 (1993).
- [22] A. Coniglio and W. Klein, *J. Phys. A* **13**, 2775 (1980).
- [23] M. E. Fisher, *Physics* **3**, 255 (1967).
- [24] R. B. Stinchcombe, in *Phase Transitions and Critical Phenomena*, edited by C. Domb and J. L. Lebowitz (Academic Press, London, 1983), Vol. 7.
- [25] B. V. Jacak *et al.*, *Phys. Rev. C* **35**, 1751 (1987).
- [26] C. A. Ogilvie *et al.*, *Phys. Rev. Lett.* **67**, 1214 (1991).
- [27] S. Das Gupta and A. Z. Mekjian, *Phys. Rep.* **72**, 131 (1981).